Inorganic Chemistry

pubs.acs.org/IC

Article

Photochromic Uranyl-Based Coordination Polymer for Quantitative and On-Site Detection of UV Radiation Dose

Jian Xie, Huiliang Hou, Huangjie Lu, Feifan Lu, Wei Liu, Xia Wang, Liwei Cheng, Yugang Zhang, Yanlong Wang, Yaxing Wang, Juan Diwu, Baowei Hu,* Zhifang Chai, and Shuao Wang*

Cite This: *Inorg. Chem.* 2023, 62, 15834−15841

Read Online

ACCESS | Metrics & More | Article Recommendations | Supporting Information

ABSTRACT: A highly sensitive detection of ultraviolet (UV) radiation is required in a broad range of scientific research, chemical industries, and health-related applications. Traditional UV photodetectors fabricated by direct wide-band-gap inorganic semiconductors often suffer from several disadvantages such as complicated manufacturing procedures, requiring multiple operations and high-cost instruments to obtain a readout. Searching for new materials or simple strategies to develop UV dosimeters for quantitative, accurate, and on-site detection of UV radiation dose is still highly desirable. Herein, a photochromic uranyl-based coordination polymer $[(UO_2)(PBPCA)\cdot DMF]\cdot DMF$ (PBPCA = pyridine-3,5-bis(phenyl-4-carboxylate), DMF = *N*,*N*′-dimethylformamide, denoted as **SXU-1**) with highly radiolytic and chemical stabilities was successfully synthesized via the solvothermal method at 100 °C. Surprisingly, the fresh samples of **SXU-1** underwent an ultra-fast UV-induced (365 nm, 2 mW) color variation from yellow to orange in less than 1 s, and then the color changed further from orange to brick red after the subsequent irradiation, inspiring us to develop a colorimetric dosimeter based on red-green-blue (RGB) parameters. The mechanism of radical-induced photochromism was intensively investigated by UV−vis absorption spectra, EPR analysis, and SC-XRD data. Furthermore, **SXU-1** was incorporated into an optoelectronic device to fabricate a novel dosimeter for convenient, quantitative, and on-site detection of UV radiation dose.

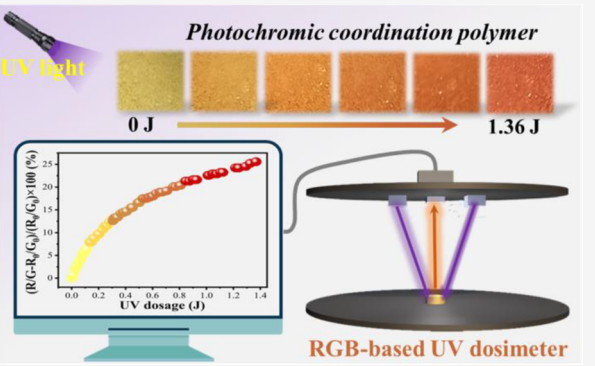

INTRODUCTION

Ultraviolet (UV) light is a common nonionizing radiation that has been broadly used in chemical industries involving photocatalysis,[1,2] curing,[3,4] photolithography,[5,6] sterilization,[7,8] and so forth. However, the exposure of human body to excessive UV doses causes a detrimental effect on skin, and this potentially incurs malignant melanoma or skin cancer.[9] At present, UV photodetectors exhibit a range of applications in health care, medicine synthesis, scientific research, space communications, and chemical sensing.[10−13] Traditional UV photodetectors, such as PIN photodiode detectors, Schottky barrier detectors, and metal−semiconductor−metal detectors, are fabricated by direct wide-band-gap inorganic semiconductors (e.g., GaN,[14] GaAsP,[15] Ga_2O_3,[16] ZnO,[17] ZnSe,[18] and ZnS[19]). Although having attracted great interests, these photodetectors often suffer from several drawbacks, including complicated and high-cost manufacturing procedures, requiring multiple operations and expensive instruments to obtain a readable output, which greatly limit their large-area applications. To tackle these issues, a great deal of effort has been devoted to developing new materials or strategies for low-cost and high-sensitive UV detection.

Photochromic materials often exhibit both reversible color changes and physicochemical property variations in response to UV or visible light, which make them draw considerable attention with their potential ability for application in fields of optical memories,[20,21] displays,[22,23] photomechanics,[24] smart windows,[25−27] photoswitches,[28,29] and so on. Generally speaking, the color of photochromic materials will undergo obvious variations with the accumulation of light irradiation dose. Such a feature makes them attractive candidates for constructing UV sensors. Typical photochromic organic molecules (e.g., diarylethene,[30,31] spiropyran[32,33] and azobenzene[34,35]) undergo isomerization upon light illumination, accompanied by reversible color changes. Moreover, viologen and its derivatives exhibit an electron-deficient nature and often combine electron donors to construct photochromic materials.[36−39] However, it is well known that purely

Received: March 24, 2023
Published: September 19, 2023

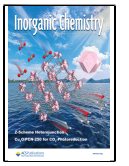

https://doi.org/10.1021/acs.inorgchem.3c00972
Inorg. Chem. 2023, 62, 15834−15841

photochromic organic molecules usually suffer from insufficient stability.[40,41] For instance, the photogenerated colored forms of these molecules are optically and thermally unstable, significantly restricting their applications in real world.[42−44] In the past two decades, numerous photochromic inorganic−organic hybrid materials, especially coordination polymers (CPs) or metal−organic frameworks (MOFs), have been developed, showing potential applications in visualized UV monitoring.[11,24,45,46] However, this type of UV detection strategy can only offer semiquantitative dose information. In addition, the reported photochromic MOFs/CPs are not sensitive enough, as they often take tens of seconds or even longer to achieve color changes when exposed to UV radiation.[47−51] Therefore, it remains a challenge to develop high-sensitive and quantitative UV dosimeters based on photochromic materials.

As the heaviest element in nature, uranium exhibits excellent optical properties and radiation absorption capacity, indicating its potential application in radiation detection. Meanwhile, depleted uranium is an abundant byproduct of nuclear industry that receives insufficient attention because of its negligible radioactivity. Lately, we spared no effort to introduce uranium into inorganic−organic hybrid materials and to validate their ability of radiation detection. Fortunately, we have prepared several uranyl-based luminescent MOFs/CPs that can detect low-dose UV, X-ray, and γ-ray down to 6.9×10^{-9} J, 1.18×10^{-5} Gy, and 1.42×10^{-5} Gy, respectively, representing the best chemical dosimeters until now.[52−55] However, luminescent methods for sensing applications usually have a non-negligible disadvantage, namely, that the luminescence intensity of sensors can be affected by temperature, humidity, as well as the condition of spectrophotometers, resulting in the reduced sensing accuracy.

Herein, we present a one-dimensional uranyl-based coordination polymer $[(UO_2)(PBPCA)\cdot DMF]\cdot DMF$ (PBPCA = pyridine-3,5-bis(phenyl-4-carboxylate), DMF = *N*,*N*′-dimethylformamide, denoted as **SXU-1**), which shows ultrasensitive UV-induced photochromism at room temperature. To solve the aforementioned drawbacks of previously reported chemical UV dosimeters, we integrated **SXU-1** into a custom-built optoelectronic device, which can directly convert the UV radiation dose to an RGB readout. Notably, five regions of linear correlations can be established between the accumulated dose and the relative increase of R/G value in the range of 0−1.36 J, realizing on-site and quantitative dose measurements. Furthermore, **SXU-1** can maintain its original crystalline structure and chemical constituents even after exposure to 12 h UV irradiation or treatment with 95% relative humidity for 12 h that enables the application of **SXU-1** in real world. Additionally, a complete decoloration of UV-irradiated samples can be achieved by a heat treatment at 100, 90, 80, and 70 °C for 5, 7, 10, and 15 h, respectively.

EXPERIMENTAL SECTION

Caution! *All uranium compounds used in these studies contained depleted uranium; standard precautions were performed for handling radioactive materials, and all studies were conducted in a laboratory dedicated to studies involving actinide elements.*

Synthesis of $[(UO_2)(PBPCA)\cdot DMF]\cdot DMF$ (SXU-1). All reagents and solvents were purchased from commercial suppliers and used as received without further purification. 0.0502 g of $UO_2(NO_3)_2\cdot 6H_2O$ (0.1 mmol), 0.0319 g of H_2PBPCA (0.1 mmol), and 5 mL of DMF were loaded into a 10 mL vial. The vial was then sealed and heated to 100 °C for 12 h and cooled to room temperature under ambient conditions. Yellowish block crystals of **SXU-1** were isolated after being washed with deionized water and allowed to air-dry at room temperature. Crystals suitable for X-ray structural analysis were collected and measured. The phase purity was confirmed by powder XRD analyses, which are shown in Figure S1. The yield of **SXU-1** was calculated to be ∼60%. Elemental analysis results: calculated C, 40.90%; N, 5.73%; H, 3.41%; found C, 40.42%; N, 5.42%; H, 3.24%.

X-ray Crystallography Studies. Single-crystal XRD (SC-XRD) data were collected at 223 K using a Turbo X-ray source (Mo Kα radiation, λ = 0.71073 Å), adopting the direct-drive rotating anode technique and a CMOS detector. The crystals were mounted on a Cryoloop with Paratone oil and optically aligned on a Bruker D8-Venture single-crystal X-ray diffractometer equipped with a digital camera. The structures were solved by direct methods and refined on F^2 by full-matrix least-squares methods using SHELXTL.[56] All nonhydrogen atoms were refined with anisotropic displacement parameters, and the carbon-bound hydrogen atoms were introduced at the calculated positions. Crystal data and structure refinement parameters are given in Table S1.

Materials and Instrumentation. The PXRD patterns were collected from 5° to 50°, with a step of 0.02° and data collection time of 0.2 s, on a Bruker D8 Advance X-ray diffractometer with Cu Kα radiation (λ = 1.54056 Å) equipped with a Lynxeye one-dimensional detector. UV−vis absorption spectra were recorded from single crystals using a Craic Technologies microspectrophotometer. Crystals were placed on quartz slides, and the data were collected after the optimization of the microspectrophotometer. The elemental analyses (C, H, and N) were carried out with a Vario EL CHNOS elemental analyzer. Infrared spectra were recorded on powdered samples using a Thermo Scientific Nicolet iS50 instrument in the range of 400−4000 cm^{-1} at room temperature. Thermogravimetric analysis (TGA) was carried out on a NETZSCH STA 449 F3 Jupiter instrument in the range of 30−900 °C under a nitrogen flow at a heating rate of 10 °C/min. The EPR data were recorded with a Bruker EMXplus 10/12 EPR spectrometer equipped with an Oxford Instruments EPR901 liquid helium continuous-flow cryostat fitted with a super-high-Q cavity. The EPR spectra of nonirradiated and irradiated samples were acquired with a sweep width of 2000 G, a frequency of 9.517216 GHz, a modulation amplitude of 5 G, a modulation frequency of 100 kHz, and at room temperature. The radiation resistance of **SXU-1** was examined by irradiating the powdery sample with UV light under ambient conditions. UV light was provided by a Xe lamp (300 W). DFT calculations were performed using the Gaussian 09 software. The study of UV sensitivity of **SXU-1** was performed on a custom-built optoelectronic device which consists of a microcontroller unit (MCU, STMicroelectronics, STM32F103C8T6) serving as a processor, a mini-USB serving as a connection port, a set of bulbs (TUOZHAN Optoelectronics, TZ35UVA + UVC02−014) for UV irradiation, and an RGB sensor (AMS, TCS34725) for signal readout.

RESULTS AND DISCUSSION

Structure Description. Single-crystal X-ray diffraction studies reveal that **SXU-1** crystallizes in the triclinic and centrosymmetric space group $P\bar{1}$. As shown in Figure 1b, the overall structure is based on charge-balanced one-dimensional uranyl-PBPCA chains. The asymmetric unit contains one crystallographically independent UO_2^{2+} ion, one $PBPCA^{2-}$ ligand, one coordinate DMF molecule, and one dissociative DMF molecule (Figure S2). The uranium(VI) center adopts a typical pentagonal bipyramidal coordination geometry with bonds to the two axial *oxo* atoms [1.758(4) and 1.747(5) Å]; four oxygen atoms come from three $PBPCA^{2-}$ [2.322(3), 2.329(4), 2.427(4), and 2.444(4) Å] and one oxygen atom from DMF [2.402(4) Å].[57] Two UO_2^{2+} ions are bridged by two independent $PBPCA^{2+}$ ligands, forming a dimer; then, two dimers are bridged by two ligands and extend into infinite charge-balanced uranyl-PBPCA chains, with coordinating DMF located on both sides of the chain (Figure 1a). The

https://doi.org/10.1021/acs.inorgchem.3c00972
Inorg. Chem. 2023, 62, 15834−15841

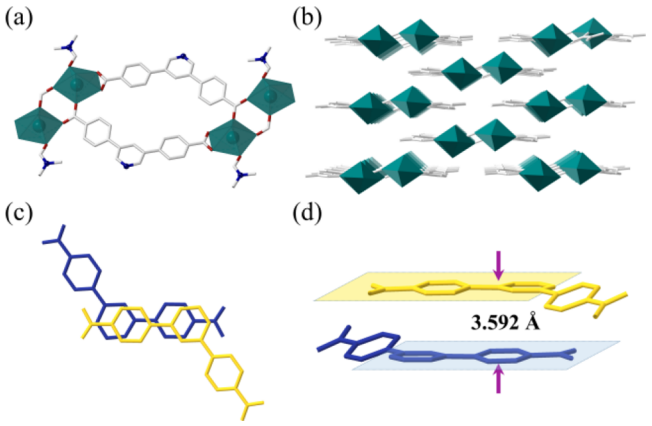

Figure 1. (a) One-dimensional uranyl-PBPCA chain. (b) Packing style of one-dimensional chains. (c) Top view showing the $\pi\cdots\pi$ interactions in the structure of **SXU-1**. (d) Side view showing the $\pi\cdots\pi$ interactions in the structure of **SXU-1**. Color scheme: U, turquoise; O, red; C, gray; N, blue. Dissociative DMF and H atoms are omitted for clarity.

distance between two $PBPCA^{2-}$ ligands on adjacent chains is 3.592 Å, indicating the presence of significant parallel π-stacking between the aromatic ring and pyridine ring of $PBPCA^{2-}$ ligands (Figure 1c,d).[58,59] Therefore, these chains are further packed via $\pi\cdots\pi$ interactions and intermolecular van der Waals interactions, as shown in Figure 1b. The thermal ellipsoid plots of crystals are shown in Figure S3.

Photochromic Properties. Generally, most of the pyridine-based MOFs/CPs are photoactive and show obvious color changes upon UV irradiation via electron transfer.[45] Similarly, photochromism property was observed in **SXU-1** which exhibits fast photochromic transformation with the exposure to UV light in the air at room temperature. Upon being irradiated by excitation light (365 nm, 2 mW) on a Craic Technologies microspectrophotometer, the fresh samples of **SXU-1** underwent a rapid and evident alteration in color from yellow to orange in less than a second, which is much shorter compared to that of the already published photochromic CPs/MOFs materials, suggesting the high sensitivity of **SXU-1** toward UV light.[60−63] To verify whether **SXU-1** is responsive to extremely weak UV light (e.g., originating from lighting lamps), we thoroughly grounded the crystals of **SXU-1** and evenly coated them on a transparent tape, which was placed in a laboratory with the lights turned on (the UV light power was measured to be 33 μW). As shown Figure S4, the coloration of **SXU-1** occurs after UV irradiation for 30 min, and the color change becomes more pronounced over time, demonstrating that **SXU-1** is also highly responsive to extremely weak UV light. The reason why **SXU-1** is highly sensitive to UV light is mainly due to the introduction of uranyl ions, which endow the material with strong absorption of UV light (Figure 2). The UV irradiation experiments of bulk samples were performed under a 300 W Xe lamp, and the irradiation time was set to 0, 1, 5, 10, 20, 60, 100, 200, and 650 s, respectively. With the increase of the irradiation time, the color of the fresh sample gradually changed from yellow to orange to brick red (the UV-induced colored sample is abbreviated as **SXU-1-UV**), and no further color change was observed after continuous irradiation for 650 s (inset of Figures 2 and S5). Generally speaking, photogenerated radicals are sensitive to oxidants, and the decoloration processes can take place under air atmosphere at

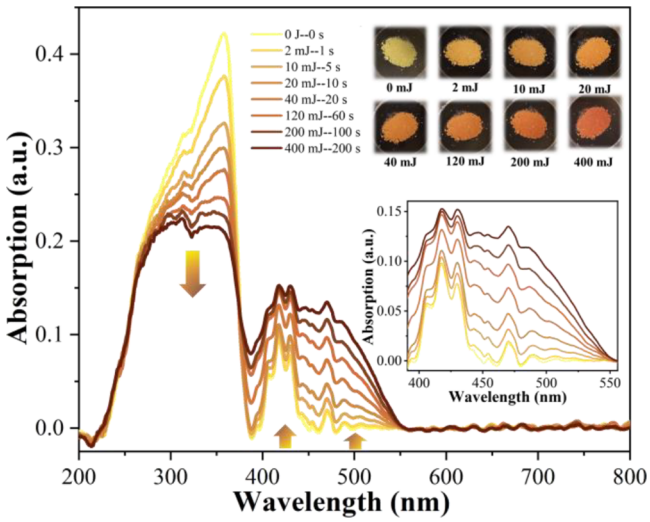

Figure 2. Evolution of the solid-state UV−vis absorption spectra of the **SXU-1** crystal after 0−400 mJ UV irradiation (365 nm, 2 mW) at room temperature. The photographs of the bulk **SXU-1** crystal after 0−400 mJ UV irradiation (300 W Xe lamp) and the solid-state UV−vis absorption spectra in the range of 390−560 nm are shown in the inset.

room temperature.[60] However, complete decoloration of **SXU-1-UV** in the air at room temperature needs over 1 year, which is mainly attributable to the dense $\pi-\pi$ stacking of the chain structure that hinders the contact of radicals with oxygen molecules. Under heating conditions, the crystal structure expands to a certain extent, promoting the entry of oxygen molecules into the interior of the material and reacting with radicals. Here, complete decoloration of **SXU-1-UV** can be easily achieved by heating at 100, 90, 80, and 70 °C for 5, 7, 10, and 15 h, respectively (Figures S6 and S7). As depicted in Figure S8, the absorption spectrum of as-synthesized **SXU-1** was collected. Based on theoretical analyses (see more details in the Supporting Information), it can be concluded that the absorption band in the range of 220−390 nm mainly consists of two electronic transition modes, namely $\pi \rightarrow \pi^*$ transitions (S1 and S2) and $n \rightarrow \pi^*$ transitions (S3) (Figure S9). In addition, the absorption band in the range of 390−500 nm mainly arises from the typical electronic transitions of UO_2^{2+}, namely, $(\sigma_u^+)^2 \rightarrow \sigma_u^+\delta_u$ and $(\sigma_u^+)^2 \rightarrow \sigma_u^+\varphi_u$ (Figure S8).[64] As shown in Figure 2, the time-dependent UV−vis absorption spectra for a single crystal of **SXU-1** were collected under exposure to 365 nm UV light. Figure 2 demonstrates that a new absorption band emerges between 500 and 560 nm, the intensity of absorption band between 390 and 500 nm increases, and the absorption band in the range of 220−390 nm diminishes gradually as a function of irradiation time. To understand the evolution of these absorption bands, the UV−vis spectra of an undeprotonated ligand (referred to as LH_2) before and after UV irradiation were collected. As shown in Figure S10, a new absorption band appears between 360 and 500 nm, which is likely attributed to the absorption by N radicals. This is because the oxygen atom in the protonated carboxyl group cannot undergo electron transfer and form oxygen radicals. Therefore, we can reasonably infer that the evolution of absorption bands in the range of 390−500 and 500−560 nm in the UV−vis absorption spectra of the UV-irradiated sample is attributed to the appearance of N and O radicals, respectively. Here, the above speculation was

https://doi.org/10.1021/acs.inorgchem.3c00972
Inorg. Chem. 2023, 62, 15834−15841

confirmed by EPR measurements. As illustrated in Figure S11, **SXU-1-UV** shows an intensive signal and a weak signal, with g factor values of 2.018 and 2.006, respectively. Additionally, 2 h of UV-irradiated LH_2 shows a signal with g factor of 2.006, which is attributed to N radicals (Figure S11). Consequently, the intensive and weak EPR signals of **SXU-1-UV** can be assigned to O radicals and N radicals, respectively.[55,65−67]

Structural Variation. The detailed structural information before and after UV irradiation was compared. The SC-XRD data reveal that both **SXU-1** and **SXU-1-UV** belong to the $P\bar{1}$ space group, while the cell parameters show slight changes (Table S1). Although the PXRD patterns of **SXU-1** and **SXU-1-UV** exhibit no obvious transformation (Figure S1), a local structural adjustment induced by photogenerated radicals was detected: (1) the PBPCA ligand underwent a certain distortion, leading to the changes of the dihedral angles between the pyridine ring and adjacent aromatic rings from 25.26 to 23.98° and 5.12 to 5.61°, respectively (Figure 3a); (2) the delocalization of radicals in the conjugated pyridine ring resulted in a significant variation of bond lengths and angles; in detail, bond lengths of C8−C9, C9−N1, and C13-C8 increased from 1.381(8) to 1.394(11) Å, 1.323(8) to 1.338(11) Å, and 1.397(7) to 1.408(10) Å, respectively; bond lengths of N1−C11 and C12−C13 decreased from 1.330(8) to 1.319(11) Å and 1.372(7) to 1.355(10) Å, respectively; bond angles of ∠C9−N1−C11, ∠C11−C12−C13, and ∠C12−C13−C8 increased from 116.5(6) to 117.7(8)°, 116.1(5) to 116.4(7)°, and 121.6(5) to 122.2(7)°, respectively; bond angles of ∠C13−C8−C9, ∠C8−C9−N1, and ∠N1−C11−C12 decreased from 115.6(5) to 115.3(7)°, 124.8(5) to 123.3(7)°, and 125.4(6) to 125.1(8)°, respectively (Figure 3b,c, Table S2s and S3); (3) the oxygen atom of carboxylate as an electron donor lost an electron during the photochromic process, contributing to the changes of bond lengths and angles of C−O; in detail, bond lengths of C20−O7 increased from 1.256(6) to 1.267(9) Å and that of C20−O6 decreased from 1.266(7) to 1.257(9) Å; the bond angle of ∠O6−C20−O7 decreased from 119.1(5) to 118.6(6)° (Figure 3b,c, Tables S2 and S3, 4) unexpectedly, the average U≡O bond length of uranyl shrinked from 1.753 to 1.735 Å, which may be caused by a weakened bond between uranium and equatorial oxygen atoms after electron transfer (Figure 3b,c, Table S2). To our best understanding, the local structural variation described here is unusual in those reported UV-induced photochromic materials where the structural change is too imperceptible to be identified after UV irradiation.

Radiolytic and Chemical Stabilities. Radiolytic and chemical stabilities are essential for the radiation dosimeter applied in real world. The radiolytic stability of **SXU-1** was studied by exposing polycrystalline **SXU-1** under UV light (300 W Xe lamp). PXRD and FTIR studies reveal that **SXU-1** can maintain its original crystalline structure and chemical constituents even after 12 h of UV irradiation, indicating the high radiolytic stability of **SXU-1** (Figures 4a and S12). Generally, the structures of one-dimensional coordination polymers are regarded as unstable. In this case, the radiolytic stability of **SXU-1** could be attributed to the robust bonds between the uranyl and organic ligand and the significant $\pi-\pi$ stacking between the two parallel uranyl-PBPCA chains. Owing to such structure features, **SXU-1** also exhibits remarkable moisture and thermal stabilities. As shown in Figure 4b, PXRD studies uncover that no obvious transformation of crystalline structure is observed when exposed to different relative humidity (RH) conditions (55, 75, and 95%) for 12 h. Moreover, thermogravimetric analysis (TGA) demonstrates that **SXU-1** shows suitable thermal stability and can maintain its structure up to 160 °C (Figure S13). To further verify the stability of **SXU-1**, we selected two well-formed single crystals which were subjected to different treatments, including exposure to 95% humidity for 12 h and 12 h of UV irradiation. Then, SC-XRD data of the two single crystals were collected. In addition, the UV-irradiated crystal was heated at 80 °C for 10 h, and its SC-XRD data were collected again. Finally, the reliable SC-XRD data can demonstrate the stability of **SXU-1** (see more details in the Supporting Information).

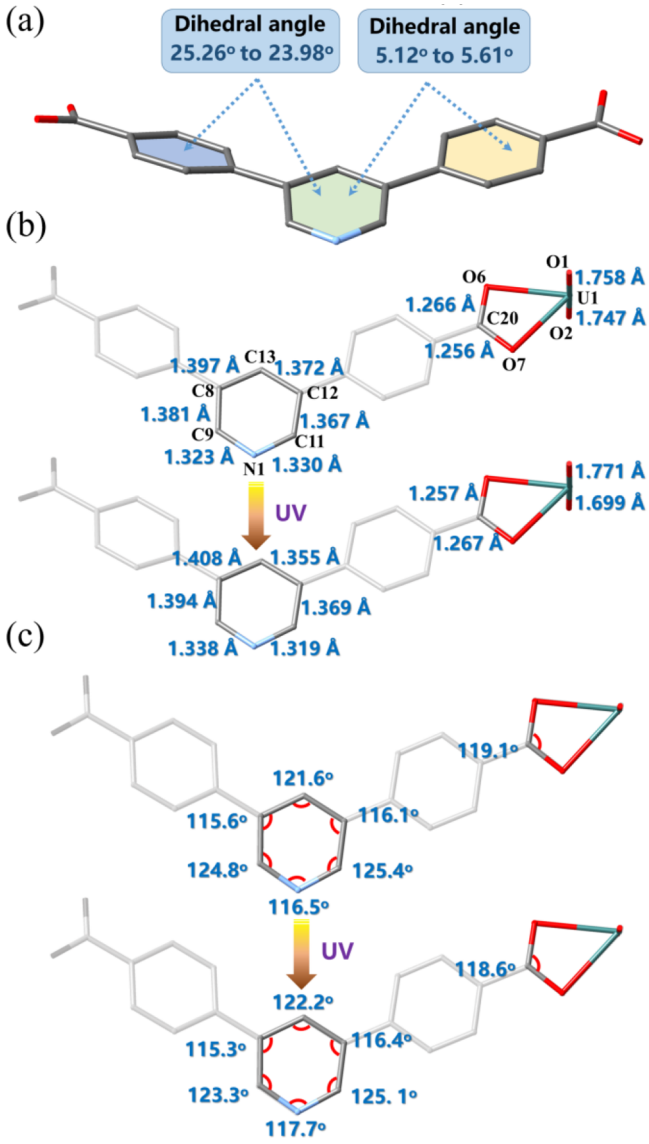

Figure 3. Local structural changes of **SXU-1** and **SXU-1-UV**. (a) Dihedral angles between the pyridine ring and adjacent aromatic rings, (b) bond lengths of C−C, C−N, C−O, and U≡O, and (c) ∠C−C−C, ∠C−N−C, and ∠C−C−N angles of pyridine ring and ∠C−O−C angle of carboxylate.

UV Dosimeter Based on SXU-1. Taking the advantage of the observable color evolution of crystals upon the accumulated radiation dose, **SXU-1** can be used as a colorimetric dosimeter for the visualized detection of UV

https://doi.org/10.1021/acs.inorgchem.3c00972
Inorg. Chem. 2023, 62, 15834−15841

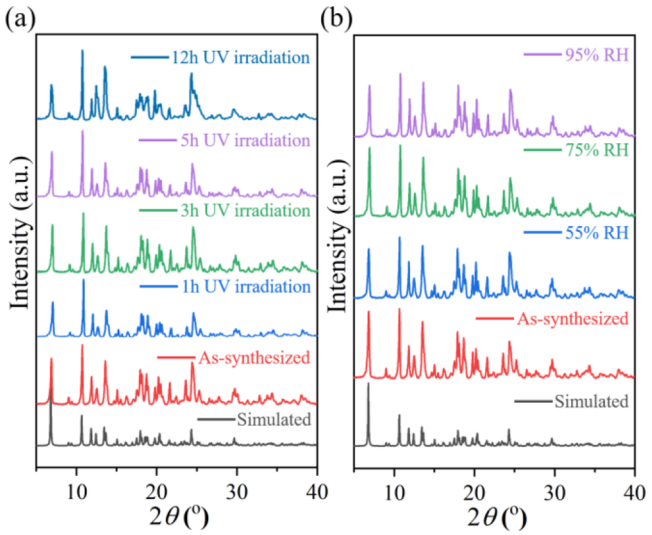

Figure 4. (a) Powder XRD patterns of nonirradiated and UV-irradiated **SXU-1**. (b) Powder XRD patterns of **SXU-1** exposed to different RH conditions.

radiation. However, such a strategy for the detection of radiation dose is semiquantitative and cannot meet the demand for an accurate dose determination. To tackle this issue, a novel RGB-based dosimeter was developed using a custom-built optoelectronic device integrating with **SXU-1** as a radiation-sensitive component in the present work.[65] As shown in Figure 5a, the top of the device (outer diameter of 5 cm) is a signal collector, and the bottom is a sample holder. The outside of the top part is equipped with a microcontroller unit (MCU, STMicroelectronics, STM32F103C8T6), and a mini-USB serves as a processor and a connection port, respectively. A set of bulbs (TUOZHAN Optoelectronics, TZ35UVA + UVC02−014) for UV irradiation and an RGB sensor (AMS, TCS34725) for readout are embedded on the inside of the top part. In addition, the bottom part of the device served as a sample holder placed vertically below the RGB sensor. Before the measurement of the UV dose, finely ground **SXU-1** (30 mg) was pressed into a tablet (with a diameter of 6 mm) as the radiation-sensitive component which was loaded on the sample holder at the bottom of the device. With continuously being irradiated by the UV radiation (30 mJ/s·cm^2), the colorimetric profile of **SXU-1** was captured and converted into an RGB readout synchronously (Figure 5b). Figure 5c demonstrates the relative increase of the R/G value as a function of the accumulated dose (0−1.36 J) of UV radiation, where R_0/G_0 is the initial measured value, and R/G is the value measured after UV irradiation. Obviously, there are five regions showing linear responses, with the R^2 values ranging from 0.986 to 0.992. As shown in Figures S15 and S16, the regeneration and repeatability experiments exhibit good reproducibility. Therefore, this device can provide a digital readout of the RGB color value for a real-time and accurate measurement of UV dose.

CONCLUSIONS

In summary, a photosensitive coordination polymer, **SXU-1**, with excellent photochromism properties was synthesized via

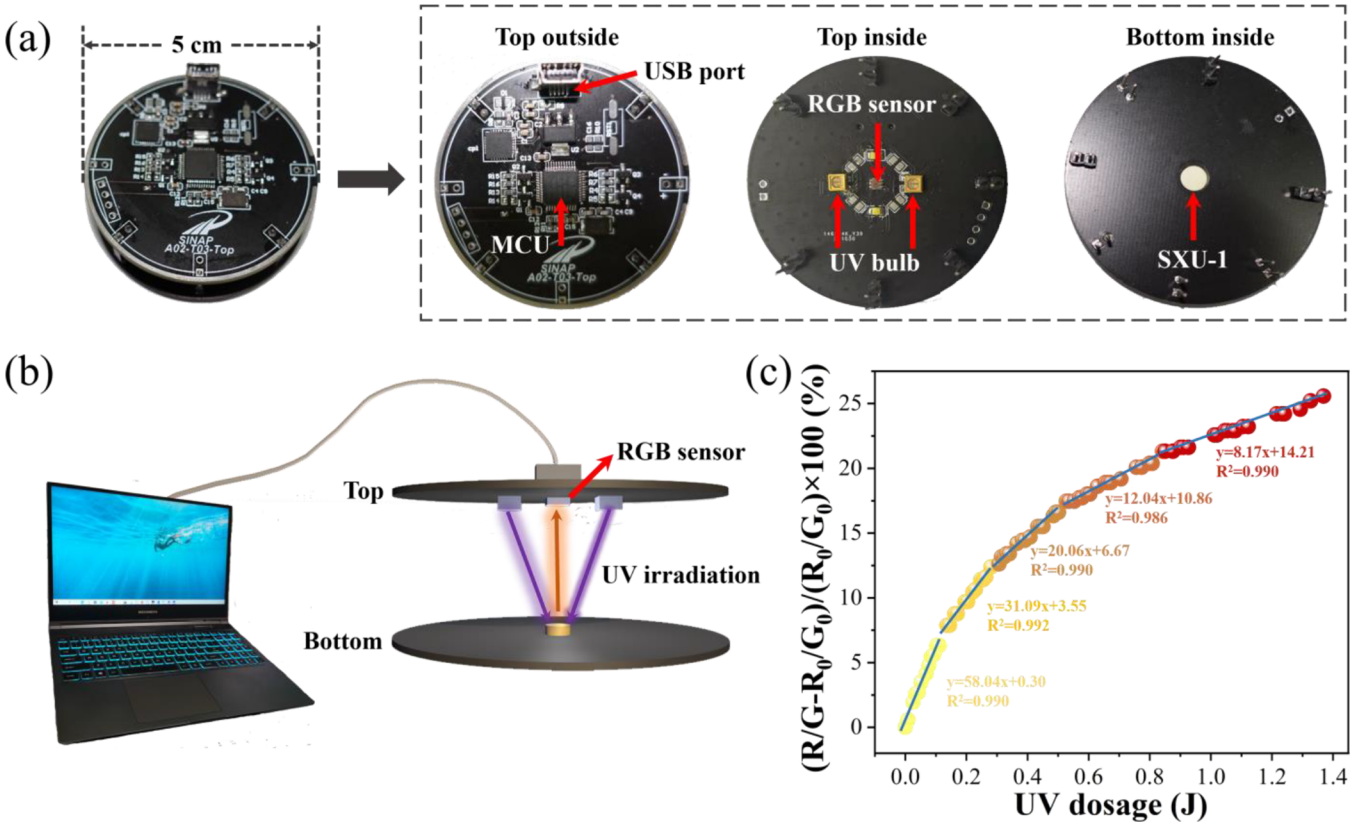

Figure 5. (a) Photographs of the RGB-based dosimeter developed using a custom-built optoelectronic device integrating with **SXU-1** as a radiation-sensitive component. (b) Schematic illustration exhibiting the operating principle of the dosimeter for on-site UV detection. (c) Relative increase of R/G value of **SXU-1** as that versus UV radiation dose.

https://doi.org/10.1021/acs.inorgchem.3c00972
Inorg. Chem. 2023, 62, 15834−15841

the self-assembly of uranyl ions and PBPCA ligands under solvothermal conditions. Remarkably, the fresh samples of **SXU-1** underwent an ultrafast UV-induced color variation from yellow to orange in less than 1 s, making **SXU-1** a splendid photoresponsive material for monitoring the UV radiation dose. The mechanism of radical-induced photochromism was intensively studied by UV−vis absorption, EPR, and SC-XRD. To overcome the qualitative nature of the previously developed photochromic UV sensors, we introduced **SXU-1** into a custom-built device which can directly convert the UV dose to an RGB readout and realized on-site UV radiation detection. Notably, this is the first case so far to develop a UV dosimeter by integrating a uranyl-bearing photochromic material into an optoelectronic device. Furthermore, the high radiolytic and chemical stabilities of **SXU-1** make it possible for real-world application.

■ ASSOCIATED CONTENT

Supporting Information

The Supporting Information is available free of charge at https://pubs.acs.org/doi/10.1021/acs.inorgchem.3c00972.

Crystallographic data, PXRD patterns, UV−vis absorption spectrum, DFT calculations, FTIR spectra, EPR spectra, optical images of **SXU-1**, and TGA data (PDF)

Accession Codes

CCDC 2232596, 2254340, 2284919−2284920, and 2284930 contain the supplementary crystallographic data for this paper. These data can be obtained free of charge via www.ccdc.cam.ac.uk/data_request/cif, or by emailing data_request@ccdc.cam.ac.uk, or by contacting The Cambridge Crystallographic Data Centre, 12 Union Road, Cambridge CB2 1EZ, UK; fax: +44 1223 336033.

■ AUTHOR INFORMATION

Corresponding Authors

Baowei Hu − *School of Life Science, Shaoxing University, Shaoxing 312000, China;* orcid.org/0000-0002-3636-2586; Email: hbw@usx.edu.cn

Shuao Wang − *State Key Laboratory of Radiation Medicine and Protection, School of Radiological and Interdisciplinary Sciences (RAD-X), Collaborative Innovation Center of Radiation Medicine of Jiangsu Higher Education Institutions, Soochow University, Suzhou 215123, China;* orcid.org/0000-0002-1526-1102; Email: shuaowang@suda.edu.cn

Authors

Jian Xie − *School of Life Science, Shaoxing University, Shaoxing 312000, China*

Huiliang Hou − *Key Laboratory of Interfacial Physics and Technology, Shanghai Institute of Applied Physics, Chinese Academy of Sciences, Shanghai 201800, China; University of Chinese Academy of Sciences, Beijing 100049, China*

Huangjie Lu − *Key Laboratory of Interfacial Physics and Technology, Shanghai Institute of Applied Physics, Chinese Academy of Sciences, Shanghai 201800, China; University of Chinese Academy of Sciences, Beijing 100049, China;* orcid.org/0000-0002-0423-2760

Feifan Lu − *School of Life Science, Shaoxing University, Shaoxing 312000, China*

Wei Liu − *School of Environmental and Material Engineering, Yantai University, Yantai 264005, China;* orcid.org/0000-0001-5034-8951

Xia Wang − *School of Environmental and Material Engineering, Yantai University, Yantai 264005, China*

Liwei Cheng − *State Key Laboratory of Radiation Medicine and Protection, School of Radiological and Interdisciplinary Sciences (RAD-X), Collaborative Innovation Center of Radiation Medicine of Jiangsu Higher Education Institutions, Soochow University, Suzhou 215123, China*

Yugang Zhang − *State Key Laboratory of Radiation Medicine and Protection, School of Radiological and Interdisciplinary Sciences (RAD-X), Collaborative Innovation Center of Radiation Medicine of Jiangsu Higher Education Institutions, Soochow University, Suzhou 215123, China*

Yanlong Wang − *State Key Laboratory of Radiation Medicine and Protection, School of Radiological and Interdisciplinary Sciences (RAD-X), Collaborative Innovation Center of Radiation Medicine of Jiangsu Higher Education Institutions, Soochow University, Suzhou 215123, China*

Yaxing Wang − *State Key Laboratory of Radiation Medicine and Protection, School of Radiological and Interdisciplinary Sciences (RAD-X), Collaborative Innovation Center of Radiation Medicine of Jiangsu Higher Education Institutions, Soochow University, Suzhou 215123, China;* orcid.org/0000-0002-1842-339X

Juan Diwu − *State Key Laboratory of Radiation Medicine and Protection, School of Radiological and Interdisciplinary Sciences (RAD-X), Collaborative Innovation Center of Radiation Medicine of Jiangsu Higher Education Institutions, Soochow University, Suzhou 215123, China;* orcid.org/0000-0002-2500-8696

Zhifang Chai − *State Key Laboratory of Radiation Medicine and Protection, School of Radiological and Interdisciplinary Sciences (RAD-X), Collaborative Innovation Center of Radiation Medicine of Jiangsu Higher Education Institutions, Soochow University, Suzhou 215123, China*

Complete contact information is available at: https://pubs.acs.org/10.1021/acs.inorgchem.3c00972

Notes

The authors declare no competing financial interest.

■ ACKNOWLEDGMENTS

This work was supported by Research Start-up Fund of Shaoxing University (13011001002/142); the Postdoctoral Science Foundation of China (2021M702387); The Science Foundation of Jiangsu Province (BK20200102); and Natural Science Foundation of the Higher Education Institutions of Jiangsu Province (22KJA150006).

■ REFERENCES

(1) Gao, C.; Wang, J.; Xu, H. X.; Xiong, Y. J. Coordination chemistry in the design of heterogeneous photocatalysts. *Chem. Soc. Rev.* **2017**, *46*, 2799−2823.

(2) Yu, Y.; Wen, W.; Qian, X. Y.; Liu, J. B.; Wu, J. M. UV and visible light photocatalytic activity of Au/TiO_2 nanoforests with Anatase/Rutile phase junctions and controlled Au locations. *Sci. Rep.* **2017**, *7*, 41253.

(3) Han, Y. H.; Taylor, A.; Mantle, M. D.; Knowles, K. M. UV curing of organic-inorganic hybrid coating materials. *J. Sol-Gel Sci. Technol.* **2007**, *43*, 111−123.

(4) Stropp, J. P.; Wolff, U.; Kernaghan, S.; Löffler, H.; Osterhold, M.; Thomas, H. UV curing systems for automotive refinish applications. *Prog. Org. Coat.* **2006**, *55*, 201−205.

(5) Guijt, R. M.; Breadmore, M. C. Maskless photolithography using UV LEDs. *Lab Chip* **2008**, *8*, 1402−1404.

(6) Hemanth, S.; Anhøj, T. A.; Caviglia, C.; Keller, S. S. Suspended microstructures of epoxy based photoresists fabricated with UV photolithography. *Microelectron. Eng.* **2017**, *176*, 40−44.
(7) Gayán, E.; Álvarez, I.; Condón, S. Inactivation of bacterial spores by UV-C light. *Innov. Food Sci. Emerg.* **2013**, *19*, 140−145.
(8) Luo, W.; Chen, A.; Chen, M.; Dong, W.; Hou, X. Comparison of sterilization efficiency of pulsed and continuous UV light using tunable frequency UV system. *Innov. Food Sci. Emerg.* **2014**, *26*, 220−225.
(9) Savona, M. R.; Jacobsen, M.; James, R.; Owen, M. Ultraviolet radiation and the risks of cutaneous malignant melanoma and non-melanoma skin cancer: perceptions and behaviours of Danish and American adolescents. *Eur. J. Cancer Prev.* **2005**, *14*, 57−62.
(10) Gedamu, D.; Paulowicz, I.; Kaps, S.; Lupan, O.; Wille, S.; Haidarschin, G.; Mishra, Y. K.; Adelung, R. Rapid Fabrication Technique for Interpenetrated ZnO Nanotetrapod Networks for Fast UV Sensors. *Adv. Mater.* **2013**, *26*, 1541−1550.
(11) Hu, S.; Zhang, J.; Chen, S.; Dai, J.; Fu, Z. Efficient Ultraviolet Light Detector Based on a Crystalline Viologen-Based Metal-Organic Framework with Rapid Visible Color Change under Irradiation. *ACS Appl. Mater. Interfaces* **2017**, *9*, 39926−39929.
(12) Monroy, E.; Omnes, F.; Calle, F. Wide-bandgap semiconductor ultraviolet photodetectors. *Semicon. Sci. Technol.* **2003**, *18*, R33.
(13) Zhou, C.; Ai, Q.; Chen, X.; Gao, X.; Liu, K.; Shen, D. Ultraviolet photodetectors based on wide bandgap oxide semiconductor films. *Chin. Phys. B* **2019**, *28*, No. 048503.
(14) Goswami, L.; Aggarwal, N.; Verma, R.; Bishnoi, S.; Husale, S.; Pandey, R.; Gupta, G. Graphene Quantum Dot-Sensitized ZnO-Nanorod/GaN-Nanotower Heterostructure-Based High-Performance UV Photodetectors. *ACS Appl. Mater. Interfaces* **2020**, *12*, 47038−47047.
(15) Park, M. S.; Jain, V.; Lee, E. H.; Kim, S. H.; Pettersson, H.; Wang, Q.; Song, J. D.; Choi, W. J. InAs/GaAs p-i-p quantum dots-in-a-well infrared photodetectors operating beyond 200 K. *Electron. Lett.* **2014**, *50*, 1731−1733.
(16) Chen, Y.; Lu, Y.; Liao, M.; Tian, Y.; Liu, Q.; Gao, C.; Yang, X.; Shan, C. 3D Solar-Blind Ga_2O_3 Photodetector Array Realized Via Origami Method. *Adv. Funct. Mater.* **2019**, *29*, No. 1906040.
(17) Yin, B.; Zhang, H.; Qiu, Y.; Luo, Y.; Zhao, Y.; Hu, L. The light-induced pyro-phototronic effect improving a ZnO/NiO/Si heterojunction photodetector for selectively detecting ultraviolet or visible illumination. *Nanoscale* **2017**, *9*, 17199−17206.
(18) Lin, T. K.; Chang, S. J.; Chiou, Y. Z.; Wang, C. K.; Chang, S. P.; Lam, K. T.; Sun, Y. S.; Huang, B. R. Homoepitaxial ZnSe MIS photodetectors with SiO_2 and BST insulator layers. *Solid-State Electron.* **2006**, *50*, 750−753.
(19) Rai, S. C.; Wang, K.; Ding, Y.; Marmon, J. K.; Bhatt, M.; Zhang, Y.; Zhou, W. L.; Wang, Z. L. Piezo-phototronic Effect Enhanced UV/Visible Photodetector Based on Fully Wide Band Gap Type-II ZnO/ZnS Core/Shell Nanowire Array. *ACS Nano* **2015**, *9*, 6419−6427.
(20) Koroteev, N. I.; Magnitskii, S. A.; Tarasishin, A. V.; Zheltikov, A. M. High-density three-dimensional optical data storage with photonic band-gap structures. *Laser Phys.* **1999**, *9*, 1253−1259.
(21) Kawata, S.; Kawata, Y. Three-Dimensional Optical Data Storage Using Photochromic Materials. *Chem. Rev.* **2000**, *100*, 1777−1788.
(22) Yang, Y. Q.; Guan, L.; Gao, G. H. Low-Cost, Rapidly Responsive, Controllable, and Reversible Photochromic Hydrogel for Display and Storage. *ACS Appl. Mater. Interfaces* **2018**, *10*, 13975−13984.
(23) Hirayama, R.; Shiraki, A.; Naruse, M.; Nakamura, S.; Nakayama, H.; Kakue, T.; Shimobaba, T.; Ito, T. Optical Addressing of Multi-Colour Photochromic Material Mixture for Volumetric Display. *Sci. Rep.* **2016**, *6*, 31543.
(24) Beery, D.; Stanisauskis, E.; McLeod, G. M.; Das, A.; Guillory, G. A.; Kennemur, J. G.; Oates, W. S.; Hanson, K. Enabling Lower Energy Light Harvesting in Stilbene-Based Photomechanical Polymers via Triplet Sensitization. *ACS Appl. Polym. Mater.* **2022**, *4*, 4081−4086.
(25) Ke, Y.; Chen, J.; Lin, G.; Wang, S.; Zhou, Y.; Yin, J.; Lee, P. S.; Long, Y. Smart Windows: Electro-, Thermo-, Mechano-, Photochromics, and Beyond. *Adv. Energy Mater.* **2019**, *9*, No. 1902066.
(26) Kim, M.; Park, K. J.; Seok, S.; Ok, J. M.; Jung, H. T.; Choe, J.; Oh, D. H.; Kim, D. H. Fabrication of Microcapsules for Dye-Doped Polymer-Dispersed Liquid Crystal-Based Smart Windows. *ACS Appl. Mater. Interfaces* **2015**, *7*, 17904−17909.
(27) Tseng, H. Y.; Chang, L.-M.; Lin, K.-W.; Li, C. C.; Lin, W. H.; Wang, C. T.; Lin, C. W.; Liu, S. H.; Lin, T. H. Smart Window with Active-Passive Hybrid Control. *Materials* **2020**, *13*, 4137.
(28) Bhattacharyya, S.; Maity, M.; Chowdhury, A.; Saha, M. L.; Panja, S. K.; Stang, P. J.; Mukherjee, P. S. Coordination-Assisted Reversible Photoswitching of Spiropyran-Based Platinum Macrocycles. *Inorg. Chem.* **2020**, *59*, 2083−2091.
(29) Zhang, Z.; Wang, W.; O'Hagan, M.; Dai, J.; Zhang, J.; Tian, H. Stepping Out of the Blue: From Visible to Near-IR Triggered Photoswitches. *Angew.Chem., Int. Ed.* **2022**, *61*, No. e202205758.
(30) Zhang, Z. X.; He, L. J.; Feng, J.; Liu, X. J.; Zhou, L.; Zhang, H. J. Unveiling the Relationship between Energy Transfer and the Triplet Energy Level by Tuning Diarylethene within Europium(III) Complexes. *Inorg. Chem.* **2020**, *59*, 661−668.
(31) Fetoh, A.; Cosquer, G.; Morimoto, M.; Irie, M.; El-Gammal, O.; El-Reash, G. M. A.; Breedlove, B. K.; Yamashita, M. Synthesis, Structures, and Magnetic Properties of Two Coordination Assemblies of Mn(III) Single Molecule Magnets Bridged via Photochromic Diarylethene Ligands. *Inorg. Chem.* **2019**, *58*, 2307−2314.
(32) Feuerstein, T. J.; Müller, R.; Barner-Kowollik, C.; Roesky, P. W. Investigating the Photochemistry of Spiropyran Metal Complexes with Online LED-NMR. *Inorg. Chem.* **2019**, *58*, 15479−15486.
(33) Yamaguchi, T.; Maity, A.; Polshettiwar, V.; Ogawa, M. Negative Photochromism Based on Molecular Diffusion between Hydrophilic and Hydrophobic Particles in the Solid State. *Inorg. Chem.* **2018**, *57*, 3671−3674.
(34) Tanimura, K.; Gon, M.; Tanaka, K. Effects of Hypervalent Bismuth on Electronic Properties of the Azobenzene Tridentate Ligand and Roles of Lewis Acidity in Controlling Optical Properties. *Inorg. Chem.* **2023**, *62*, 4590−4597.
(35) Mehrparvar, S.; Scheller, Z. N.; Wölper, C.; Haberhauer, G. Design of Azobenzene beyond Simple On-Off Behavior. *J. Am. Chem. Soc.* **2021**, *143*, 19856−19864.
(36) Berville, M.; Karmazin, L.; Wytko, J. A.; Weiss, J. Viologen cyclophanes: redox controlled host-guest interactions. *Chem. Commun.* **2015**, *51*, 15772−15775.
(37) Courtois, J.; Wang, B.; Abdul-Hassan, W. S.; Almásy, L.; Yan, M.; Royal, G. Redox-Responsive Colloidal Particles Based on Coordination Polymers Incorporating Viologen Units. *Inorg. Chem.* **2020**, *59*, 6100−6109.
(38) Wang, P. H.; Liu, B. W.; Wang, G. Q.; Sun, C. Photochromic Semiconductors: Bottom-Up Strategy to Construct Type II-Stacking Viologen π-Aggregates. *Inorg. Chem.* **2022**, *61*, 17196−17201.
(39) Xu, G.; Guo, G. C.; Wang, M. S.; Zhang, Z. J.; Chen, W. T.; Huang, J. S. Photochromism of a methyl viologen bismuth(III) chloride: structural variation before and after UV irradiation. *Angew. Chem., Int. Ed.* **2007**, *46*, 3249−3251.
(40) Rath, B. B.; Vittal, J. J. Single-Crystal-to-Single-Crystal [2 + 2] Photocycloaddition Reaction in a Photosalient One-Dimensional Coordination Polymer of Pb(II). *J. Am. Chem. Soc.* **2020**, *142*, 20117−20123.
(41) Takami, S.; Kuroki, L.; Irie, M. Photochromism of mixed crystals containing bisthienyl-, bisthiazolyl-, and bisoxazolylethene derivatives. *J. Am. Chem. Soc.* **2007**, *129*, 7319−7326.
(42) Arai, R.; Uemura, S.; Lrie, M.; Matsuda, K. Reversible Photoinduced Change in Molecular Ordering of Diarylethene Derivatives at a SolutionHOPG Interface. *J. Am. Chem. Soc.* **2008**, *130*, 9371−9379.
(43) Inaba, K.; Iwai, R.; Morimoto, M.; Irie, M. Thermally reversible photochromism of dipyrrolylethenes. *Photochem. Photobiol. Sci.* **2019**, *18*, 2136−2141.

https://doi.org/10.1021/acs.inorgchem.3c00972
Inorg. Chem. 2023, 62, 15834−15841

(44) Liu, Z.; Wang, H. I.; Narita, A.; Chen, Q.; Mics, Z.; Turchinovich, D.; Klaui, M.; Bonn, M.; Mullen, K. Photoswitchable Micro-Supercapacitor Based on a Diarylethene-Graphene Composite Film. *J. Am. Chem. Soc.* **2017**, *139*, 9443−9446.
(45) Wang, M. S.; Xu, G.; Zhang, Z. J.; Guo, G. C. Inorganic-organic hybrid photochromic materials. *Chem. Commun.* **2010**, *46*, 361−376.
(46) Xu, G.; Guo, G. C.; Guo, J. S.; Guo, S. P.; Jiang, X. M.; Yang, C.; Wang, M. S.; Zhang, Z. J. Photochromic inorganic-organic hybrid: a new approach for switchable photoluminescence in the solid state and partial photochromic phenomenon. *Dalton Trans.* **2010**, *39*, 8688−8692.
(47) Chen, H.; Zheng, G.; Li, M.; Wang, Y.; Song, Y.; Han, C.; Dai, J.; Fu, Z. Photo- and thermo-activated electron transfer system based on a luminescent europium organic framework with spectral response from UV to visible range. *Chem. Commun.* **2014**, *50*, 13544−13546.
(48) Li, H. Y.; Xu, H.; Zang, S. Q.; Mak, T. C. A viologen-functionalized chiral Eu-MOF as a platform for multifunctional switchable material. *Chem. Commun.* **2016**, *52*, 525−528.
(49) Li, H. Y.; Wei, Y. L.; Dong, X. Y.; Zang, S. Q.; Mak, T. C. W. Novel Tb-MOF Embedded with Viologen Species for Multi-Photofunctionality: Photochromism, Photomodulated Fluorescence, and Luminescent pH Sensing. *Chem. Mater.* **2015**, *27*, 1327−1331.
(50) Qiu, X. T.; Shi, Q.; Zhang, D. Q.; Lin, Q. F.; Sun, Y. Q. A Multi-Responsive Cd-Viologen Complex: Photochromism, Photo-modulated Fluorescence, and Luminescent Sensing. *ChemistrySelect* **2018**, *3*, 6611−6616.
(51) Sun, J. K.; Cai, L. X.; Chen, Y. J.; Li, Z. H.; Zhang, J. Reversible luminescence switch in a photochromic metal-organic framework. *Chem. Commun.* **2011**, *47*, 6870−6872.
(52) Liu, W.; Dai, X.; Xie, J.; Silver, M. A.; Zhang, D.; Wang, Y.; Cai, Y.; Diwu, J.; Wang, J.; Zhou, R.; Chai, Z.; Wang, S. Highly Sensitive Detection of UV Radiation Using a Uranium Coordination Polymer. *ACS Appl. Mater. Interfaces* **2018**, *10*, 4844−4850.
(53) Xie, J.; Wang, Y.; Liu, W.; Liang, C.; Zhang, Y.; Chen, L.; Sheng, D.; Chai, Z.; Wang, S. A uranyl based coordination polymer showing response to low-dosage ionizing radiations down to 10^{-5} Gy. *Sci. China: Chem.* **2020**, *63*, 1608−1612.
(54) Xie, J.; Wang, Y.; Liu, W.; Yin, X.; Chen, L.; Zou, Y.; Diwu, J.; Chai, Z.; Albrecht-Schmitt, T. E.; Liu, G.; Wang, S. Highly Sensitive Detection of Ionizing Radiations by a Photoluminescent Uranyl Organic Framework. *Angew. Chem., Int. Ed.* **2017**, *56*, 7500−7504.
(55) Xie, J.; Wang, Y.; Zhang, D.; Liang, C.; Liu, W.; Chong, Y.; Yin, X.; Zhang, Y.; Gui, D.; Chen, L.; Tong, W.; Liu, Z.; Diwu, J.; Chai, Z.; Wang, S. Photo-exfoliation of a highly photo-responsive two-dimensional metal-organic framework. *Chem. Commun.* **2019**, *55*, 11715−11718.
(56) Sheldrick, G. M. *SHELXTL*; Siemens Analytical X-ray Instruments: Madison, WI, 2001.
(57) Ji, J. Y.; Qi, C.; Zhao, H. X.; Yan, X. W.; Chai, Z. F.; Wang, S. A.; Zheng, T. Regulating the Porosity of Uranyl Phosphonate Frameworks with Quaternary Ammonium: Structure, Characterization, and Fluorescent Temperature Sensors. *Inorg. Chem.* **2022**, *61*, 16794−16804.
(58) Wang, Y. L.; Liu, Z. Y.; Li, Y. X.; Bai, Z. L.; Liu, W.; Wang, Y. X.; Xu, X. M.; Xiao, C. L.; Sheng, D. P.; Diwu, J.; Su, J.; Chai, Z. F.; Albrecht-Schmitt, T. E.; Wang, S. A. Umbellate Distortions of the Uranyl Coordination Environment Result in a Stable and Porous Polycatenated Framework That Can Effectively Remove Cesium from Aqueous Solutions. *J. Am. Chem. Soc.* **2015**, *137*, 6144−6147.
(59) Wang, X.; Wang, Y. L.; Dai, X.; Silver, M. A.; Liu, W.; Li, Y. X.; Bai, Z. L.; Gui, D. X.; Chen, L. H.; Diwu, J.; Zhou, R. H.; Chai, Z. F.; Wang, S. A. Phase transition triggered aggregation-induced emission in a photoluminescent uranyl-organic framework. *Chem. Commun.* **2018**, *54*, 627−630.
(60) Wang, J.; Li, S. L.; Zhang, X. M. Photochromic and Nonphotochromic Luminescent Supramolecular Isomers Based on Carboxylate-Functionalized Bipyridinium Ligand: (4,4)-Net versus Interpenetrated (6,3)-Net. *ACS Appl. Mater. Interfaces* **2016**, *8*, 24862−24869.
(61) Hu, S. Z.; You, M. L.; Chen, S. H.; Fu, Z. Y. A fast-response photochromic host-guest coordination polymer with a close-packed stacking structure. *CrystEngComm* **2016**, *18*, 7221−7224.
(62) Li, W. B.; Chen, X. H.; Chen, J. Z.; Huang, R.; Ye, J. W.; Chen, L.; Wang, H. P.; Yang, T.; Tang, L. Y.; Bai, J.; Mo, Z. W.; Chen, X. M. Photochromic Metal-Organic Framework for High-Resolution Inkless and Erasable Printing. *ACS Appl. Mater. Interfaces* **2022**, *14*, 8458−8463.
(63) Gao, Z. N.; Feng, D. X.; Wang, Y.; Li, F. H.; Sun, H. Y.; Hu, J. X.; Wang, G. M. Large Room Temperature Magnetization Enhancement in a Copper-Based Photoactive Metal-Organic Framework. *Inorg. Chem.* **2022**, *61*, 15812−15816.
(64) Servaes, K.; Hennig, C.; Deun, R. V.; Görller-Walrand, C. Structure of $[UO_2Cl_4]^{2-}$ in Acetonitrile. *Inorg. Chem.* **2005**, *44*, 7705−7707.
(65) Lu, H. J.; Hou, H. L.; Hou, Y. C.; Zheng, Z. F.; Ma, Y. Y.; Zhou, Z. Y.; Guo, X. F.; Pan, Q. J.; Wang, Y. G.; Qian, Y.; Wang, J. Q.; Lin, J. A New Concept of Radiation Detection Based on a Fluorochromic and Piezochromic NanoclusterA New Concept of Radiation Detection Based on a Fluorochromic and Piezochromic Nanocluster. *J. Am. Chem. Soc.* **2022**, *144*, 3449−3457.
(66) Lu, H. J.; Xie, J.; Wang, X. Y.; Wang, Y. X.; Li, Z. J.; Diefenbach, K.; Pan, Q. J.; Qian, Y.; Wang, J. Q.; Wang, S. A.; Lin, J. Visible colorimetric dosimetry of UV and ionizing radiations by a dual-module photochromic nanocluster. *Nat. Commun.* **2021**, *12*, 2798.
(67) Guo, P. Y.; Sun, C.; Zhang, N. N.; Cai, L. Z.; Wang, M. S.; Guo, G. C. An inorganic-organic hybrid photochromic material with fast response to hard and soft X-rays at room temperature. *Chem. Commun.* **2018**, *54*, 4525−4528.

https://doi.org/10.1021/acs.inorgchem.3c00972
Inorg. Chem. 2023, 62, 15834−15841